J. Ocean Univ. China (Oceanic and Coastal Sea Research)
https://doi.org/10.1007/s11802-024-5984-3
ISSN 1672-5182, 2024 23 (6): 1677-1688
http://www.ouc.edu.cn/xbywb/
E-mail:xbywb@ouc.edu.cn

Dynamics of Haptophytes (Eukaryota, Hacrobia) Revealed *via* Short-Term Sampling in the South China Sea

ZHANG Haoyue[1), 2)], LI Ran[1), 2)], GU Bowei[1), 2)], KONG Hejun[1), 2)], XU Jie[3)], ZHANG Rui[4)], LI Xiaolin[1)], JIAO Nianzhi[1), 2)], and XU Dapeng[1), 2), *]

1) *College of Ocean and Earth Sciences*, *State Key Laboratory of Marine Environmental Science*, *Xiamen University*, *Xiamen* 361102, *China*
2) *Institute of Marine Microbes and Ecospheres*, *Fujian Key Laboratory of Marine Carbon Sequestration*, *Xiamen University*, *Xiamen* 361102, *China*
3) *Centre for Regional Oceans*, *Department of Ocean Science and Technology*, *Faculty of Science and Technology*, *University of Macau*, *Macau* 999078, *China*
4) *Institute for Advanced Study*, *Shenzhen University*, *Shenzhen* 518060, *China*

(Received May 8, 2024; revised May 14, 2024; accepted June 24, 2024)

Abstract Haptophytes (Eukaryota, Hacrobia) play a crucial role in the energy budget and element cycling of diverse aquatic ecosystems due to their ability to engage in both phototrophic and mixotrophic nutritional modes. Nevertheless, there is a significant lack of knowledge regarding the short-term variations, such as diel dynamics, of their ecological features. During a short time frame in the summer of 2018, samples were collected from three distinct water layers in the South China Sea, including surface water, the deep chlorophyll maximum (DCM) layer, and 200 m depth. Fluorescence *in situ* hybridization coupled with tyramide signal amplification was used to quantify haptophyte cell abundance. Most haptophyte communities in all three water layers were composed of cells 2–5 μm in size, while the proportion of cells <2 μm increased with water depth. High-throughput sequencing of the V4 hypervariable regions of the *SSU rRNA* revealed that *Chrysochromulina* and *Phaeocystis* predominated the community, and the former was more abundant in the surface water and 200 m depth and the latter was more abundant in the DCM layer. Higher abundance of small cells (<2 μm and 2–5 μm) during the night was found compared to the day time, whereas large cells (5–10 μm and 10–20 μm) were more prevalent during the day time. The results of correlation analyses showed that haptophyte abundance was possibly impacted by both environmental biotic (heterotrophic nanoflagellates, heterotrophic bacteria, and viruses) and abiotic (temperature, salinity, and nutrients) factors.

Key words eukaryotic phytoplankton; FISH-TSA; high-throughput sequencing; microbial eukaryotes; size fraction

1 Introduction

Haptophytes (Eukaryota, Hacrobia) are unicellular, free-living eukaryotic microalgae. They typically have two equal (or slightly unequal) flagella, and a haptonema protrudes from the anterior tip of cells (Tsuji and Yoshida, 2017). Mostly living in marine environments, haptophytes are argued to be the second or third most abundant group of eukaryotic phytoplankton and are widely distributed across oceanic regions, ranging from polar to tropical, thus constituting an indispensable constituent of marine ecosystems (Penot *et al*., 2022). According to their trophic mode, haptophytes are typically photoautotrophic or mixotrophic. Their phototrophic behavior establishes them as major primary producers within the marine microbial food web. According to Liu *et al*. (2009), haptophytes account for 20%–50% of the total chlorophyll *a* (Chl *a*) biomass in the ocean. Meanwhile, it was documented that a significant proportion of bacterivory was attributed to mixotrophic haptophytes (Unrein *et al*., 2014; Chan *et al*., 2019).

Haptophytes play an essential function not only in the marine energy budget but also in the cycling of elements such as carbon, sulfur, and nitrogen. For example, coccolithophores contribute to the global carbon cycle by generating calcium carbonate, which acts as a CO_2 source in the ocean's surface waters, and organic matter, which functions as a CO_2 sink (Reinfelder, 2011). Haptophytes are key producers of dimethylsulfoniopropionate (DMSP) in the Southern Ocean, far exceeding other phytoplankton groups (Kameyama *et al*., 2020). Certain haptophytes can host the obligate symbionts, unicellular cyanobacterial group A (UCYN-A), which can actively fix N_2 in a wide variety of oceanic habitats (Landa *et al*., 2021). The cell-specific rates of UCYN-A symbioses in the Southern California Current System ecosystem are high enough to explain the N_2 fixation of the entire community (Turk-Kubo *et al*., 2021).

It is crucial to understand the environmental driving va-

* Corresponding author. E-mail: dapengxu@xmu.edu.cn

riables and the dynamics of haptophyte ecological characteristics, such as cell abundance, biomass, cell size composition, and community structure, due to the vital ecological functions they perform in marine environments. Up until now, studies have primarily focused on either broad timescales (monthly or seasonal) dynamics of the haptophyte community (Unrein *et al*., 2014; Hu *et al*., 2018; Chan *et al*., 2019) or one-time sampling but covering broader locations (Not *et al*., 2008; Lin *et al*., 2014). It has been proposed that diel rhythm drives marine organisms to perform a sea of diel rhythmicity, especially in the euphotic zone (Morimoto *et al*., 2020). Studies also revealed that diel fluctuations of some marine microorganisms can influence biogeochemical processes in the ocean, including nitrogen fixation, sulfonate cycling, and triacylglycerol biosynthesis (Becker *et al*., 2018; Durham *et al*., 2019). However, due to logistic constraints in the sampling in the open ocean, especially when sampling covers deep waters, studies conducted on temporal scales of hours targeting haptophytes remain largely lacking. Diel rhythmicity in the metabolic activity and photosynthesis of many eukaryotic plankton groups has been observed (Hu *et al*., 2018; Lambert *et al*., 2019; Becker *et al*., 2021). In North Pacific high-nutrient, low-chlorophyll waters, the dynamics of metatranscriptomes of >5 μm pelagic microbes were revealed *via* sampling at 4 h intervals over about 2.6 days, and some haptophyte transcripts, including genes encoding translation-related proteins, histones, and axonemal complexes, also exhibited day-night periodicity (Kolody *et al*., 2019). The diel rhythmicity of eukaryotic phytoplankton is closely related to the dynamics of food webs and biogeochemical cycling (Hernández Limón *et al*., 2020). Thus, it is crucial to obtain comprehensive data on the short-term dynamics of haptophyte communities.

The present study was carried out in the South China Sea (SCS), a marginal sea located in the northwestern Pacific Ocean. A summer cruise was conducted in June 2018, during which water samples were collected every 3 h for a duration of 24 h from the deep chlorophyll maximum (DCM) layer, the surface water (5 m depth), and the 200 m depth. Additionally, measurements were conducted on various environmental parameters, including water temperature, salinity, light, nutrients (nitrate, nitrite, phosphate, ammonium, and dissolved silicate), dissolved organic carbon (DOC), Chl *a*, and picoplankton abundances, including viral-like particles, heterotrophic prokaryotes, *Synechococcus*, *Prochlorococcus*, and photosynthetic picoeukaryotes. Fluorescence *in situ* hybridization coupled with tyramide signal amplification (FISH-TSA) was used to quantify haptophyte cell numbers, and high-throughput sequencing on the V4 hypervariable regions of the *SSU rRNA* was used to determine their molecular community composition. By conducting short-term and high-frequency sampling, this study aims to reveal: 1) changes in the haptophyte abundance/biomass and cell size composition across three distinct water layers; 2) changes in the haptophyte molecular community composition; and 3) potential environmental variables that influence haptophyte communities.

2 Materials and Methods

2.1 Sample Collection and Measurement of Environmental Parameters

The sampling of diel cycle water samples followed the Eulerian time-series strategy, where samples were taken at a fixed geographic location over time (Le Bouteiller and Herbland, 1982). Samples were collected at site SCS_TM (111.32°E, 18.24°N) on June 29, 2018 (Fig.1). Seawater samples were collected at regular 3-h intervals (03:00, 06:00, 09:00, 12:00, 15:00, 18:00, 21:00, and 24:00) from three distinct depths: the surface water (5 m depth), DCM, and 200 m, using Niskin bottles that were attached in a circular rosette around the CTD sensors. *In situ* measurements were taken on salinity, temperature, and photosynthetic active radiation (PAR).

Nutrients and Chl *a* samples were obtained by filtering seawater through a 47 mm GF/F (Gleman) glass fiber filter. The filtered samples were then stored at −20℃ until analysis. Chl *a* was extracted in 90% acetone at 4℃ in the dark for 24 h after 20 min of sonication. Samples were centrifuged at 4000 r min^{-1} for 10 min and measured using a Turner Designs Model 10 fluorometer. Nutrients, including nitrate (NO_3^-), nitrite (NO_2^-), phosphate (PO_4^{3-}), ammonium (NH_4^+), and dissolved silicate (DSi), were analyzed using a Seal AA3 auto-analyzer (Bran-Luebbe, GmbH) according to Li *et al*. (2008).

2.2 FISH-TSA and Observations on Haptophytes

Seawater samples (*ca*. 200 mL) were fixed with formaldehyde (final concentration 2%) for 5–10 h, collected onto 0.8 μm pore size ISOPORE (Millipore) membranes, and stored at −20℃ for further processing. The FISH-TSA protocol followed Not *et al*. (2002) and Lin *et al*. (2014). In summary, the filters were subjected to hybridization using PRYM02 (5'-GGA ATA CGA GTG CCC CTG AC-3', Simon *et al*., 2000) and PRYM03 (5'-GTC AGG ATT CGG GCA ATT-3', Eller *et al*., 2007) probes (1:1 mixed), both of which were horseradish peroxidase-labeled, at a final concentration of 5 ng μL^{-1} in a hybridization buffer consisting of 40% deionized formamide, 0.9 mol L^{-1} NaCl, 20 mmol L^{-1} Tris-HCl, 0.01% sodium dodecyl sulfate (SDS), and 2% blocking reagent (Roche Diagnostic Boehringer). After being hybridized at 35℃ for 3 h, the filters underwent two 10-min washes at 37℃ to wash off the nonhybridized probes with a washing buffer containing 56 μmol L^{-1} NaCl, 5 mmol L^{-1} EDTA, 0.01% SDS, and 20 mmol L^{-1} Tris-HCl (pH 7.5). The signal was amplified for 30 min in the dark at room temperature using an amplification buffer that contained Alexa488-tyramide. Following the counterstaining of cellular nuclei with 4',6-diamidino-2-phenylindole (DAPI) and the mounting with a glycerol mixing antifading reagent AF3 (Citiñuor Ltd.), the filter was examined under an epi-fluorescent microscope (Olympus BX51). Under excitation at a wavelength of 470 nm (blue), the FISH signals emit a green color. Cells without the characteristic green color were designated as 'non-haptophyte cells' and were excluded from enumeration.

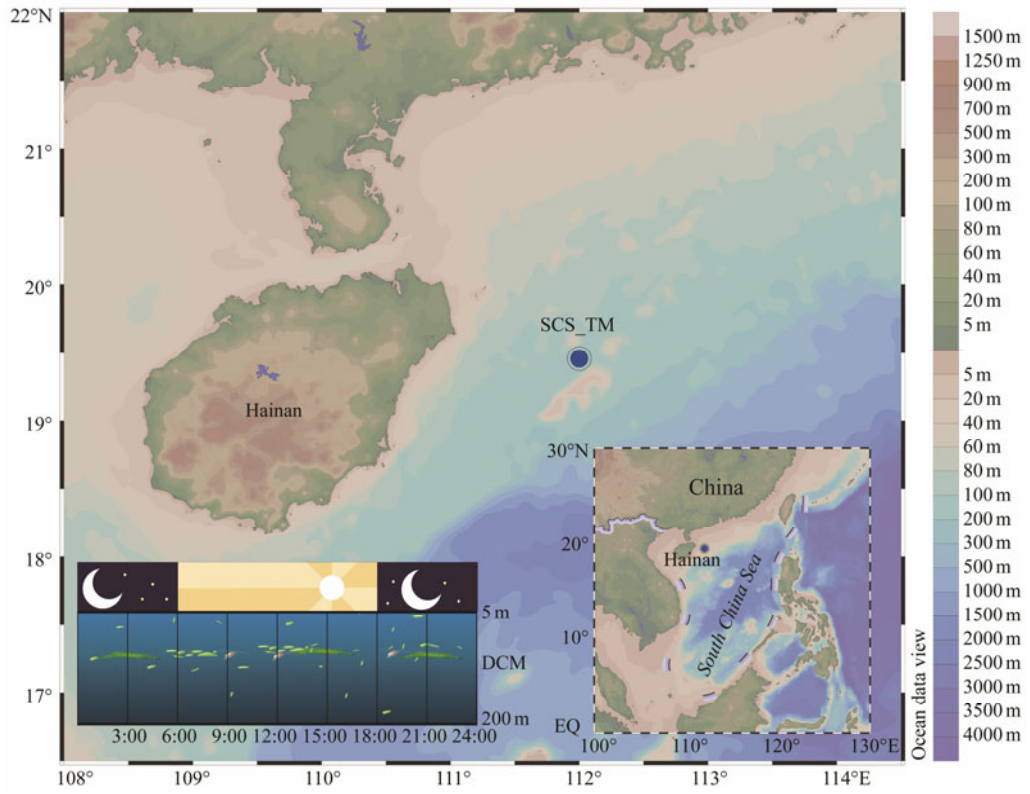

Fig.1 Location of the sampling station in the South China Sea. The sampling strategy employed in the present study is shown in the lower left corner. The map used in the figure was downloaded from http://bzdt.ch.mnr.gov.cn/index.html.

2.3 Analysis of Nanoflagellates and Picoplankton

To determine the abundance of nanoflagellate (NF), 40 mL of seawater samples were preserved in glutaraldehyde (final concentration 1%), fixed at 4℃ for 2–4 h, filtered onto black polycarbonate membrane filters with a pore size of 0.8 μm, and subsequently stained for 10 min with DAPI (final concentration 10 μg mL^{-1}). The filters were examined under an epifluorescence microscope (Olympus BX51). Pigmented nanoflagellates (PNFs) were distinguished from heterotrophic nanoflagellates (HNFs) by their red autofluorescence from chloroplasts under blue light excitation (Caron *et al*., 2017). NF were classified into three size fractions, *i.e.*, 2–3 μm, 3–5 μm, and 5–10 μm. To depict NF cell volumes, the equivalent spherical diameter was calculated using the cell's length and width. The carbon biomass of NF was estimated using a conversion factor of 0.22 pgC $μm^{-3}$ (Børsheim and Bratbak, 1987).

Flow cytometry was employed to analyze picoplankton abundance, including heterotrophic prokaryotes (HPs), *Synechococcus*, *Prochlorococcus*, photosynthetic picoeukaryotes (PPEs), and viral-like particles (VLPs). In each test of five replicates, 1.8 mL subsamples prefiltered through a 20 μm mesh (Safar) were fixed with ice-cold glutaraldehyde (final concentration 0.1%), kept at 4℃ for 20 min, flash frozen in liquid nitrogen, and then stored at −80℃ until analyses. The procedures used for flow cytometry analysis were described by Marie *et al*. (1999). To enumerate HPs, *Synechococcus*, *Prochlorococcus*, and PPEs, an Accuri C6 (Becton Dickinson, Franklin Lake, NJ, United States) was used. For the quantification of VLPs, an Epics Altra II (Beckman Coulter, Brea, CA, United States) was employed.

2.4 Nucleic Acid Extraction, PCR Amplification, High-Throughput Sequencing, and Sequence Analysis

At each depth, 2 L of seawater were prefiltered through a 200 μm mesh (Nitex) and collected onto 47-mm diameter, 0.4 μm pore size membrane (Millipore) filters. Co-extraction of total DNA and RNA was performed using the AllPrep DNA/RNA kit (Qiagen, USA), as described by Xu *et al*. (2017). Extracted RNA was reversely transcribed to cDNA using the QuantiTect® Reverse Transcription Kit (Qiagen, China), which removed residual DNA prior to the reverse transcription reaction. The universal eukaryotic primers TAReuk454FWD1 and TAReukREV3 were used to amplify the hypervariable V4 regions of the *SSU rRNA* gene (Stoeck *et al*., 2010). For each sample, four independent PCR reactions were conducted to collect enough amplicons for sequencing. PCR products for the same sample were combined and purified using the Wizard® SV Gel and PCR Clean-Up System (Promega, Beijing, China). The samples were sequenced by paired-end (2 × 250 bp) multiplexed sequencing on the Illumina MiSeq platform at a commercial company. All sequence data have been submitted to the NCBI Sequence Read Archive and are available under the accession number PRJNA1080651.

The raw data underwent quality filtering, demultiplexing, and assembling in accordance with the criteria outlined in Li *et al*. (2021) using Trimmomatic (Bolger *et al*., 2014) and Flash (Magoč and Salzberg, 2011). The quality-filtered reads were subsequently duplicated using Usearch 11

(Edgar, 2010). Following the application of Mothur screening to reads (Schloss *et al*., 2009), only those between 300 and 500 bp were retained for subsequent analysis. Using UNOISE3, reads were clustered into zero-radius OTUs (ZOTUs) after being denoised (Edgar, 2016a). An ZOTU is defined as clusters of sequences with 100% similarity (Edgar, 2016a). Taxonomy assignment on ZOTUs was conducted using SINTAX (Edgar, 2016b) against the PR2 (Protist Ribosomal Reference Database) version 4.11.1, which contains the curated haptophyte reference database (Guillou *et al*., 2012). The generation of ZOTU tables was conducted in Usearch 11, and ZOTUs not associated with Eukaryota were eliminated. The ZOTU table was then normalized at the lowest sequence counts (39116) among all samples. Only Haptophyta-affiliated ZOTUs were left in the final ZOTU table for downstream analysis.

2.5 Statistical Analysis

Based on Spearman correlation analysis, the Paleontological Statistics (PAST) software (Hammer *et al*., 2001) was used to examine the relationships between the abundance of total and size-fractionated haptophyte and the measured environmental parameters, including water temperature, salinity, PAR, nutrients (NO_3^-, NO_2^-, PO_4^{3-}, NH_4^+, and DSi), DOC, Chl *a*, and microbial abundances, including VLPs, HPs, *Synechococcus*, *Prochlorococcus*, PPEs, and HNFs.

3 Results

3.1 Environmental Parameters

Throughout the sampling period, variations in most environmental variables were negligible at each of the three water depths, respectively (Fig.2). The water temperature declined as the water depth increased, whereas the salinity demonstrated an inverse relationship. The concentrations of DSi, NO_3^-, and PO_4^{3-}, increased with the increasing water depth. There was no statistically significant variation observed in the concentration of NH_4^+ across the three layers, which ranged 0.1–0.25 μmol L^{-1}. As water depth increased, DOC concentrations decreased marginally from 70 μmol L^{-1} at the surface water, 60 μmol L^{-1} at the DCM layer, to 50 μmol L^{-1} at 200 m depth. As expected, clear diel changes of light were found in the surface water and DCM layer, but not at the 200 m depth. In the surface water, Chl *a* was marginally higher in the day than at the night. At the DCM layer and 200 m depth, Chl *a* was relatively stable and low, with a peak at 12:00 at 200 m depth.

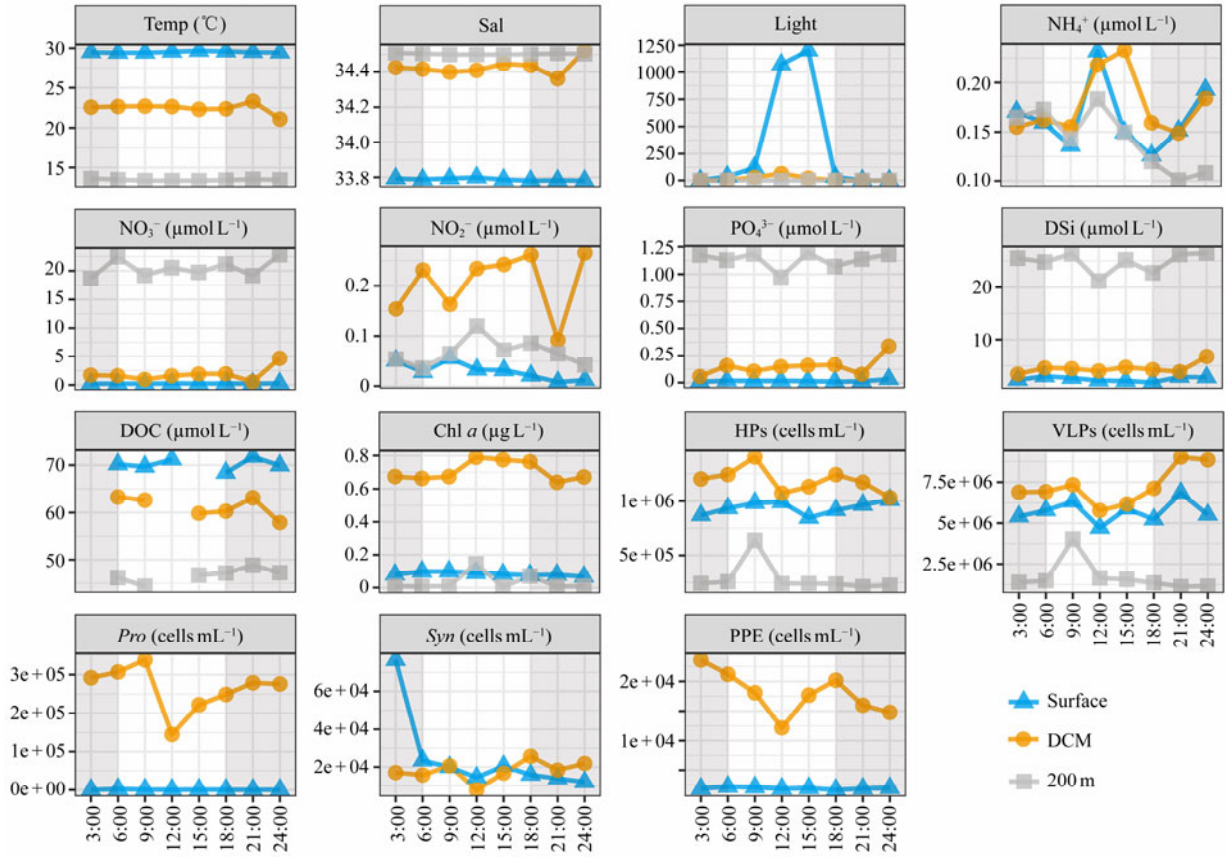

Fig.2 Short term changes of water temperature (Temp), salinity (Sal), light, ammonium (NH_4^+), nitrite (NO_3^-), nitrate (NO_2^-), phosphate (PO_4^{3-}), silicate (DSi), dissolved organic carbon (DOC), Chl *a*, and the abundance of heterotrophic prokaryotes (HPs), viral-like particles (VLPs), *Procholorococcus* (*Pro*), *Synechococcus* (*Syn*), and photosynthetic picoeukaryotes (PPEs) in the surface water, DCM layer, and 200 m depth, respectively.

The abundances of HPs and VLPs were the highest at the DCM layer ((1.0–1.4) × 10^6 cells mL^{-1} for HPs and (5.8–9.0) × 10^6 cells mL^{-1} for VLPs, respectively), followed by the surface water and 200 m depth. The abundance of HPs

in the DCM layer peaked at 09:00 and declined to its minimum at 24:00. Similarly, the abundance of VLPs peaked at 21:00 and declined to its minimum at 12:00. In surface water, the abundance of HPs was the highest at 24:00 and the lowest at 15:00; the abundance of VLPs was the highest at 21:00 and the lowest at 12:00, respectively. The abundances of VLPs and HPs at 200 m depth remained comparatively stable, with a peak observed at 9:00. The abundance of *Prochlorococcus* at the DCM layer ($(1.45-3.38)\times10^5$ cells mL^{-1}) was higher compared to that at the surface water ($(1.07-8.17)\times10^2$ cells mL^{-1}). The abundance of *Prochlorococcus* at the DCM layer increased from 3:00 to 9:00, then fell precipitously at 12:00 before rising again, while that at the surface water remained relatively constant. *Synechococcus* abundance did not differ substantially at both surface water ($(1.20-7.65)\times10^4$ cells mL^{-1}) and DCM layer ($(1.57-2.57)\times10^4$ cells mL^{-1}), except that a peak was observed at 3:00 at the surface water. PPEs exhibited a drop-rise-drop pattern at the DCM layer, with a substantially higher abundance at the DCM layer ($(1.22-2.02)\times10^4$ cells mL^{-1}) compared to the surface water ($(1.67-2.19)\times10^3$ cells mL^{-1}).

3.2 Temporal Variations in the Abundances and Cell Size Composition of Nanoflagellates (NFs)

NFs were separated into HNFs and PNFs, which were further divided into 3 groups with different sizes (2–3 μm, 3–5 μm, and 5–10 μm), respectively (Fig.3). Overall, the abundance of HNFs was the highest in the surface water (374–977 cells mL^{-1}), followed by the abundance in the DCM layer (132–615 cells mL^{-1}) and at the 200 m depth (96–246 cells mL^{-1}). However, there was one exception where the abundance of HNFs in the DCM layer exceeded that in certain night samples involving the 3–5 μm size group. At 24:00, the abundance of HNFs was the highest in the surface water, and it was the lowest in the 200 m depth at 6:00. The abundance of PNFs in the DCM layer is generally higher (mean ± s.e., (1431 ± 192) cells mL^{-1}) than in the surface water ((698 ± 76) cells mL^{-1}). The DCM layer experienced an initial increase from 3:00 to 6:00 in the morning, followed by a decrease from 6:00 to 9:00 pm. Following the onset of nightfall, the abundance reverted to its prior state. PNFs were barely observed in the 200 m depth ((25 ± 11) cells mL^{-1}).

The 2–3 μm size group comprised the majority of both HNFs and PNFs communities, while the 5–10 μm size fraction made a negligible contribution. Meanwhile, with the increasing water depth, the proportions of the 2–3 μm size group increased for both HNFs (*ca*. 71.9%, 62.0%, and 73.6% in the surface water, the DCM layer, and 200 m depth, respectively) and PNFs (*ca*. 67.1%, 60.2%, and 84.8% in the surface water, the DCM layer, and 200 m depth, respectively) (Fig.4).

3.3 Temporal Changes in the Abundances, Biomass, and Cell Size Composition of Haptophytes

FISH-TSA was used to differentiate haptophyte cells from other eukaryotic cells (Fig.5). The average haptophyte abundance in the surface water, DCM layer, and 200 m depth were (212 ± 54), (224 ± 54), and (46 ± 4) cells mL^{-1}, respectively. In general, the abundance of haptophytes was the highest at 3:00 at DCM layer, or 6:00 at surface water. It decreased during the day, reached the lowest at 15:00 (DCM layer) or 18:00 (surface water), and rose again during the night. The haptophyte abundance remained relatively stable at 200 m depth; however, there were marginally more haptophyte cells observed during the day compared to the night (Fig.6). The haptophyte community was mainly composed of cells 2–5 μm in size, followed by the <2 μm, 5–10 μm, and 10–20 μm size fractions. In the 200 m depth, pico-sized haptophytes (pico_HAP) typically made a greater contribution to the overall community than those in the surface water and DCM layer (Fig.7A).

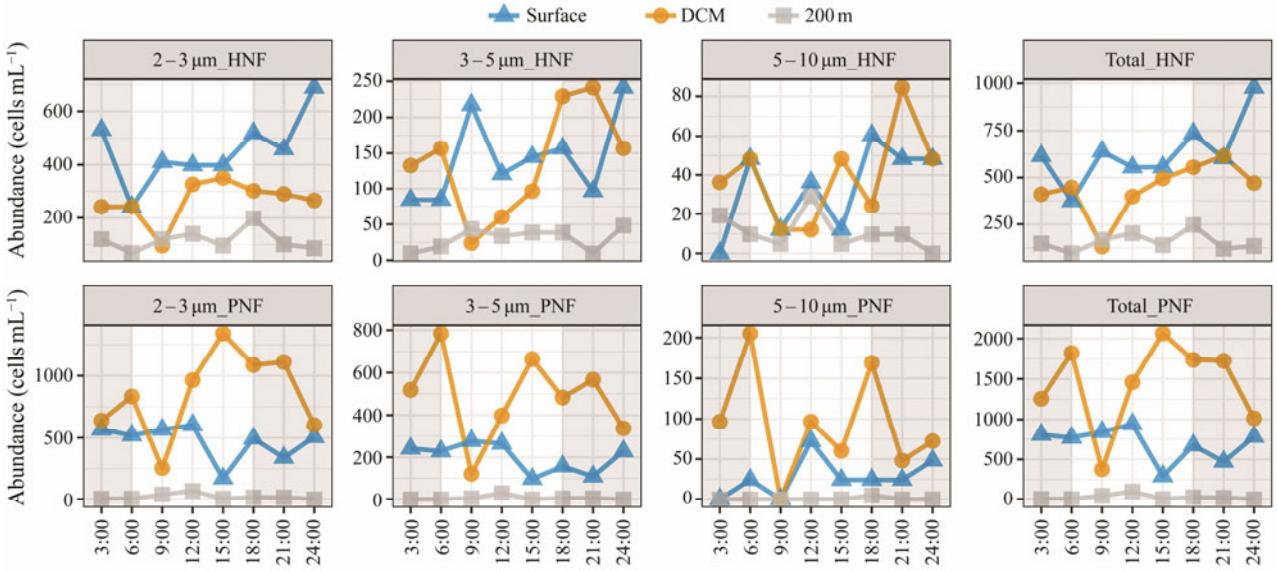

Fig.3 Temporal variations in the abundance of size fractionated and total heterotrophic nanoflagellates (HNF) and pigmented nanoflagellates (PNF).

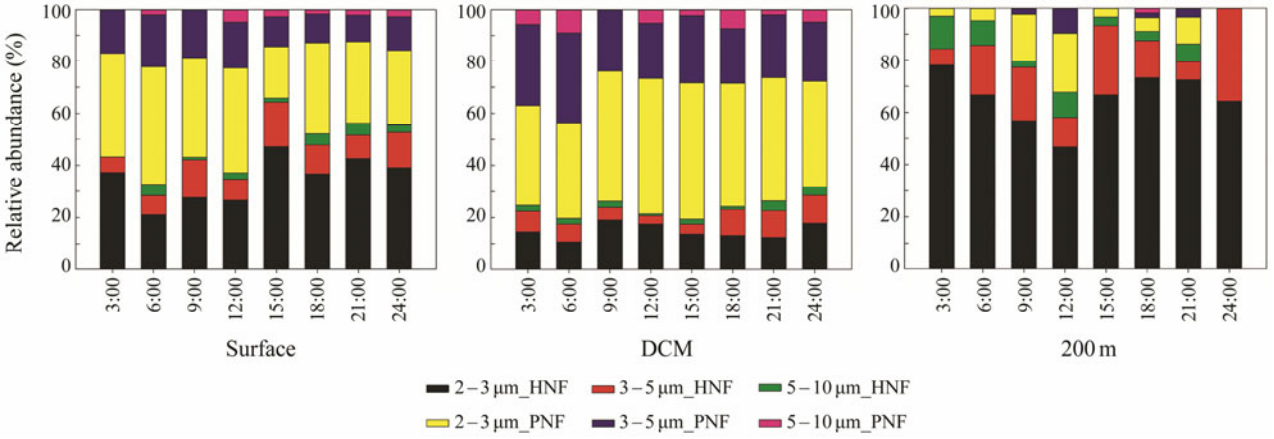

Fig.4 Abundance proportions of size fractionated nanoflagellates in the surface water, DCM layer, and 200 m depth, respectively.

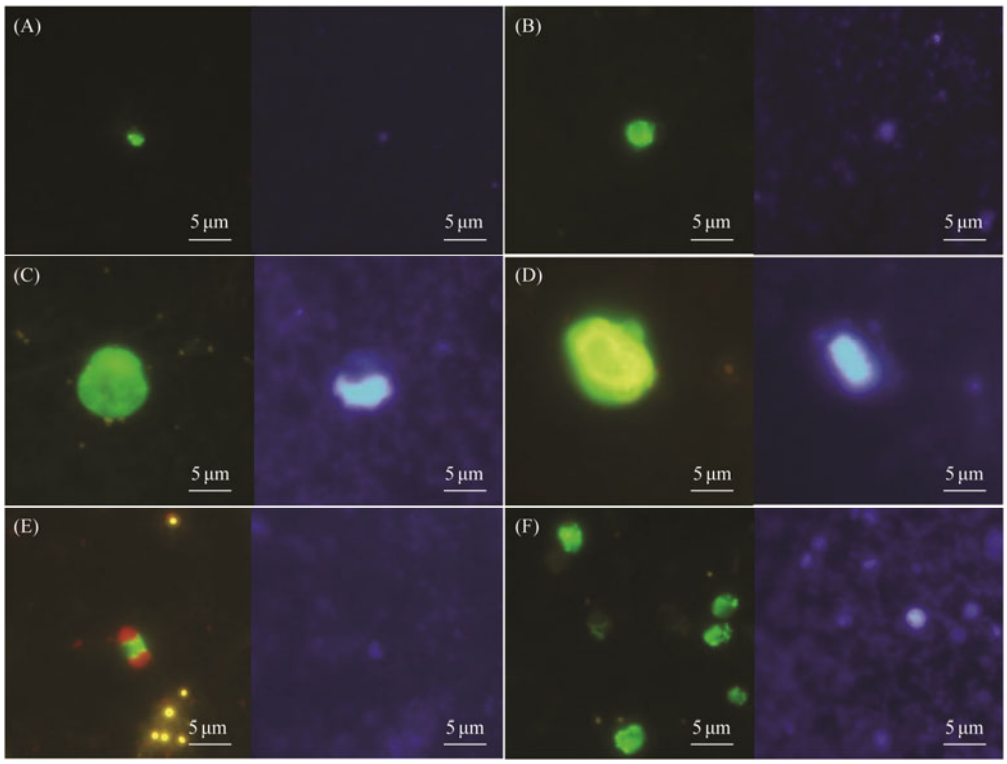

Fig.5 Haptophyte (A–E) and non-haptophyte (F) cells under blue (left) and ultraviolet lights (right), respectively.

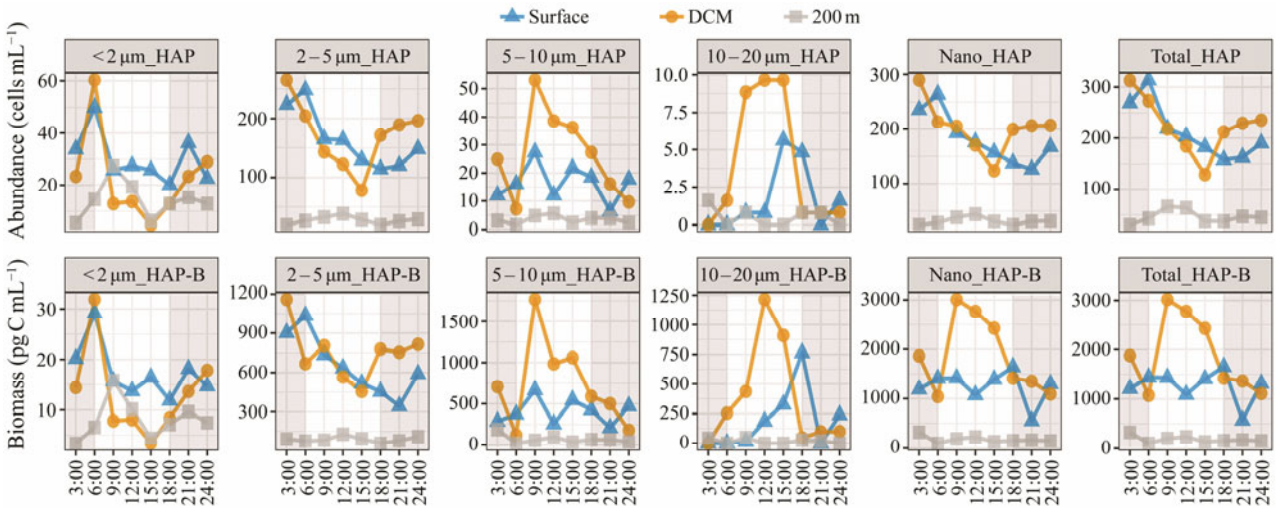

Fig.6 Temporal variations in the abundance and biomass of size fractionated and total haptophytes revealed by FISH-TSA.

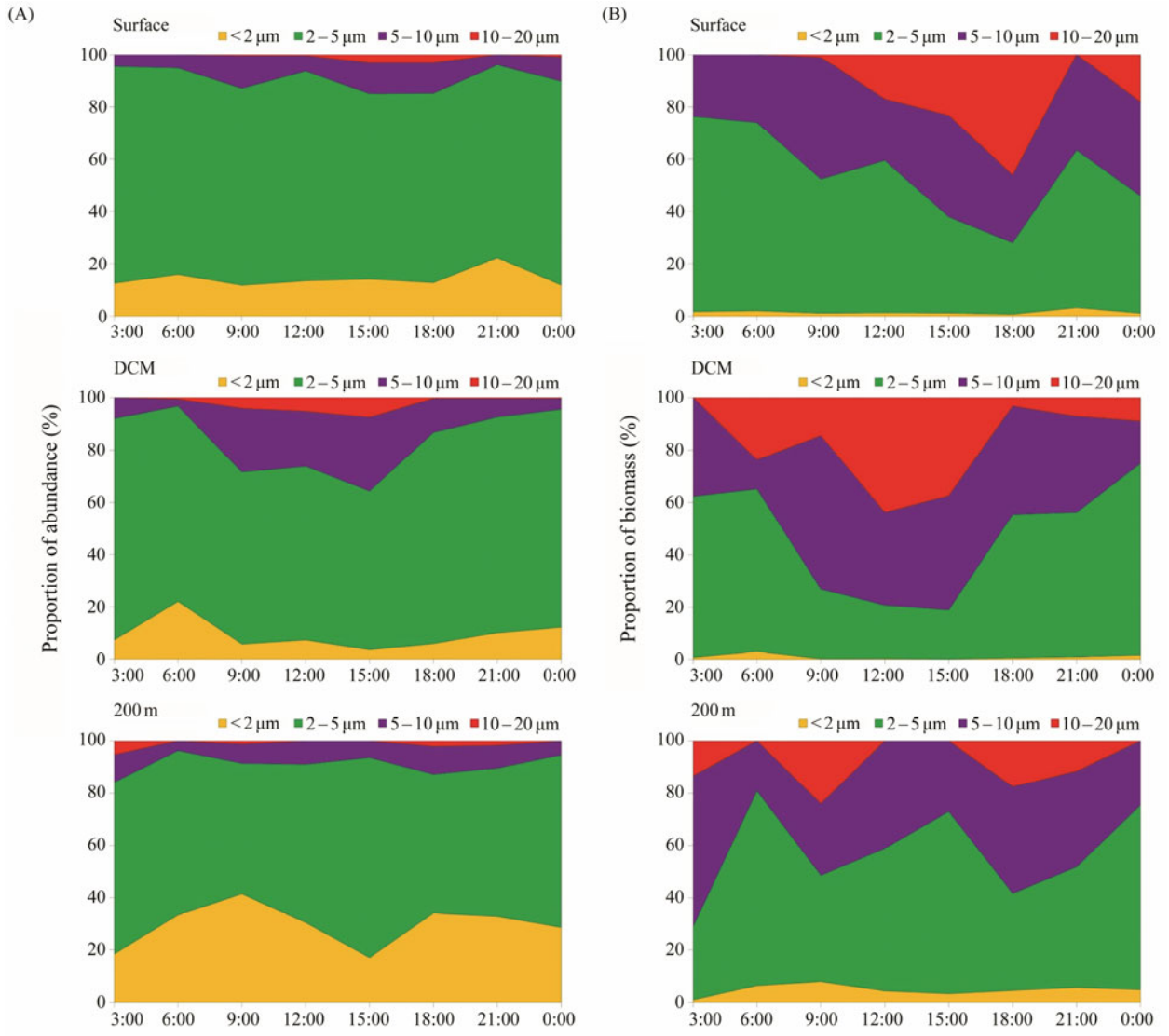

Fig.7 Abundance (A) and biomass (B) proportions of size-fractionated haptophytes to total haptophytes in the surface water, DCM layer, and 200 m depth, respectively.

In general, the carbon biomass value of total haptophytes was the highest in the DCM layer, followed by the surface water and the 200 m depth (Fig.6). No discernible diel patterns were observed in the surface water and at the 200 m depth. However, within the DCM layer, carbon biomass tended to be greater during the day compared to the night. The haptophyte biomass consisted primarily of cells 2–5 μm in size; however, in certain samples, including samples collected from 200 m depth at 3:00, DCM layer at 9:00, 5 m depth and DCM layer at 15:00, and 200 m depth at 18:00, the contribution of cells 5–10 μm in size fraction was the greatest (Fig.7B).

3.4 Temporal Changes in the Molecular Composition of Haptophyte Communities

The proportions of haptophyte-affiliated sequences to total eukaryotic sequences were 0.21%–36.05%, 0.05%–7.64%, and 0.06%–5.31% in the surface water, DCM layer, and 200 m depth, respectively. The greatest contribution in the surface water was at 21:00, while those in the DCM layer and 200 m depth were at 24:00 and 18:00, respectively.

Regardless of depth and time, the haptophyte community was dominated by the genus *Chrysochromulina*. The Phaeocystales, particularly *Phaeocystis*, comprised a greater proportion of the haptophyte communities in the DCM layer. Conversely, the 200 m depth showed a greater contribution from environmental clades, including Prymnesiophyceae_Clade_B3-E (Fig.8).

3.5 Correlations of the Abundance and Biomass of Haptophytes with Environmental Parameters

Spearman correlation analysis between haptophyte abundance and environmental variables showed the total haptophyte abundance was significantly and positively correlated with temperature, light, the abundances of VLPs and HPs, and negatively correlated with salinity, concentrations of NO_3^-, PO_4^{3-}, and DSi, and the abundance of HNFs (Table 1). However, haptophyte size groups showed distinct correlations with environmental variables. The <2 μm haptophytes were negatively correlated with salinity and nutrients, including NO_3^-, PO_4^{3-}, and DSi, while positively correlated with <5 μm HNFs. Haptophytes 2–5 μm and

5–10 μm in size exhibited similar correlations with environmental variables, with the exception that the cells 2–5 μm in size were also positively correlated with 5–10 μm HNFs, and the cells 5–10 μm in size were also positively correlated with light. The haptophytes, 10–20 μm in size, were only positively correlated with light.

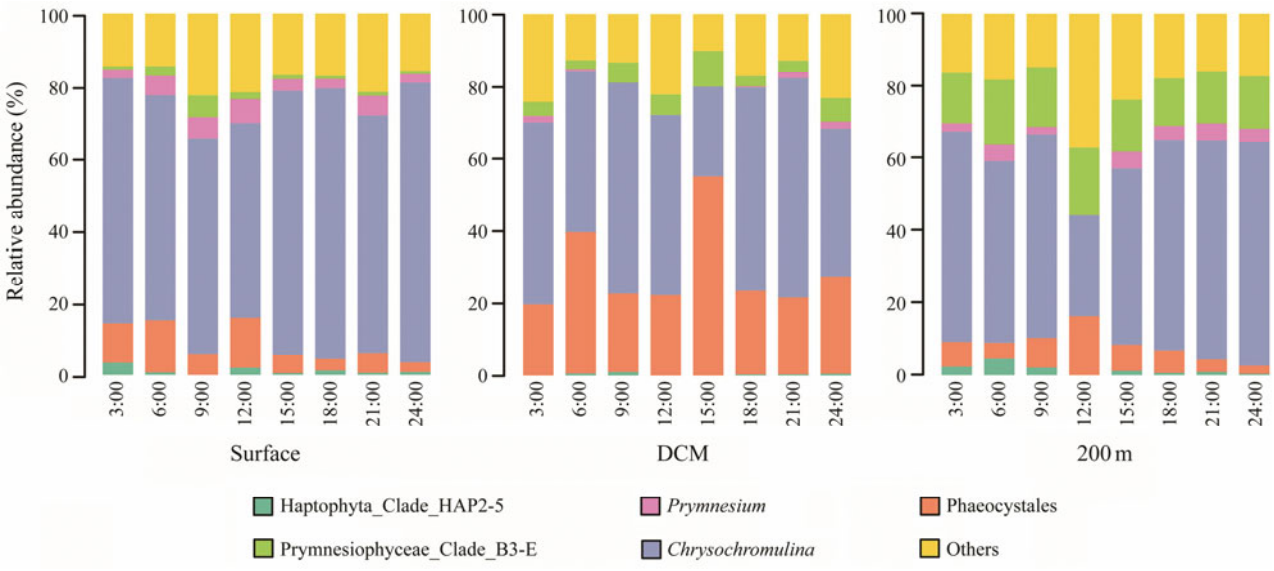

Fig.8 Temporal dynamics in the molecular composition of haptophyte communities at the surface water, DCM layer, and 200 m depth.

Table 1 Spearman correlation between environmental variables and size-fractionated haptophyte abundances

Environmental variable	<2 μm-HAP		2–5 μm-HAP		5–10 μm-HAP		10–20 μm-HAP		Nano-HAP		Total-HAP	
	R	*P*	R	*P*	R	*P*	R	*P*	R	*P*	R	*P*
HNF	0.433	0.035	**0.555**	**0.005**	**0.523**	**0.009**			0.482	0.017	0.482	0.017
2–3 μm HNF	0.424	0.039	0.490	0.015	**0.561**	**0.004**			0.431	0.036	0.431	0.036
3–5 μm HNF	0.427	0.037	**0.689**	**<0.001**	**0.532**	**0.007**			**0.615**	**0.001**	**0.615**	**0.001**
>5 μm HNF			0.455	0.025					0.434	0.034	0.434	0.034
Chl *α*			**0.638**	**0.001**	**0.792**	**<0.001**			**0.682**	**<0.001**	**0.682**	**<0.001**
NH_4^+												
$NO_3^- + NO_2^-$	**−0.577**	**0.003**	**−0.619**	**0.001**	**−0.602**	**0.002**			**−0.604**	**0.002**	**−0.604**	**0.002**
NO_2^-												
NO_3^-	−0.576	**0.003**	**−0.634**	**0.001**	**−0.612**	**0.001**			**−0.622**	**0.001**	**−0.622**	**0.001**
PO_4^{3-}	**−0.555**	**0.005**	**−0.630**	**0.001**	**−0.606**	**0.002**			**−0.613**	**0.001**	**−0.613**	**0.001**
DSi	−0.487	0.016	**−0.622**	**0.001**	**−0.635**	**0.001**			**−0.589**	**0.002**	**−0.589**	**0.002**
Light					**0.703**	**<0.001**	0.507	0.011	0.410	0.047	0.410	0.047
Temperature	0.512	0.010	**0.568**	**0.004**	**0.576**	**0.003**			**0.550**	**0.005**	**0.550**	**0.005**
Salinity	−0.452	0.027	−0.506	0.012	**−0.568**	**0.004**			−0.481	0.017	−0.481	0.017
HPs			**0.720**	**<0.001**	**0.761**	**<0.001**			**0.746**	**<0.001**	**0.746**	**<0.001**
VLPs			**0.770**	**<0.001**	**0.689**	**<0.001**			**0.782**	**<0.001**	**0.782**	**<0.001**

Notes: Numbers in bold indicated $P<0.01$ and numbers underlined indicated $P<0.05$. Blank indicated non-significant correlations.

4 Discussion

4.1 Dynamics of Haptophyte Abundance and Size Fraction Composition

Haptophyte cells were conventionally classified into either pico- or nano-size fractions (Cuvelier *et al*., 2010; Masquelier *et al*., 2011). Although environmental sequencing coupled with haptophyte-specific primers revealed a huge diversity of pico-sized haptophytes (Liu *et al*., 2009; Edvardsen *et al*., 2016; Sun *et al*., 2022), FISH-TSA showed that nano-sized haptophytes were generally more abundant than pico-sized cells (Not *et al*., 2005; Liu *et al*., 2009; Unrein *et al*., 2014). For example, in some areas, no haptophytes <2 μm were found (Marie *et al*., 2010). At an oligotrophic coastal site, 73% of the haptophytes sampled from 5 m depth were 3–5 μm in size, 21% were 5–20 μm, and only 6% were <3 μm (Unrein *et al*., 2014). In the subtropical western Pacific Ocean, cells <3 μm and 3–5 μm accounted for *ca*. 17% and 57% of all haptophytes, respectively (Chan *et al*., 2019). In a study that sampled haptophytes in North Pacific, Mediterranean Sea, and North Atlantic waters, *ca*. 75% of haptophytes ranged between 3 and 5 μm (Liu *et al*., 2009). The current investigation involved the separation of haptophytes into two fractions: < 2 μm (pico) and 2–20 μm (nano), the latter of which was further subdivided into 2–5 μm, 5–10 μm, and 10–20 μm. The total abundance of haptophyte cells was (212.3±19.2)

(mean ± s.e.), (224.3 ± 19.5), and (46.4 ± 4.4) cells mL^{-1} in the surface water, the DCM, and 200 m depth, respectively. A small proportion of the total haptophyte abundance in the surface water (*ca*. 14.3%) and DCM layer (*ca*. 9.4%) was attributed to cells <2 μm. The haptophyte abundance in the surface water ((1.6–3.1) × 10^2 cells mL^{-1}, averaging 2.2 × 10^2 cells mL^{-1}) found in the present study is consistent with previous reports. For example, haptophyte abundance in summer surface water (2 to 3 m depth) of the East China Sea ranged from 4.8 × 10^1 to 3.1 × 10^3 cells mL^{-1}, with an average of 6 × 10^2 cells mL^{-1}, which was higher than the present study (Lin *et al*., 2014). The wider range of haptophyte abundance found in Lin *et al*. (2014) may be explained by their broader sampling area. An annual investigation conducted at a coastal site in the Mediterranean revealed that the abundance of pico-sized haptophytes fluctuated around 40 cells mL^{-1}, whereas nano-sized haptophytes consistently surpassed 300 cells mL^{-1} (average: 804 cells mL^{-1}) (Unrein *et al*., 2014). The higher haptophyte abundance observed by Unrein *et al*. (2014) may be caused by the higher latitudinal location of their sampling site, which is consistent with previous findings, indicating that haptophytes are generally more abundant in high latitude areas (Endo *et al*., 2018). Higher haptophyte abundance was found in the oligotrophic coastal waters of northern Taiwan, China, where the annual average abundance of haptophytes in the surface water was (465 ± 121.56) cells mL^{-1}, peaking in July (*ca*. 1173 cells mL^{-1}) (Chan *et al*., 2019).

In the present study, haptophytes <2 μm and 2–5 μm in size were found to be more abundant at night compared to the day in the surface water and DCM layer. During the day, the abundance decreased from 6:00 to 15:00, increased during the day-night transition from 18:00, and then continued to rise during the night. This elevated abundance observed during the night may be ascribed to the characteristic synchronous reproductive pattern of haptophytes. In contrast to Bacillariophyceae, the majority of haptophyte cell division occurs only at night (Mas *et al*., 2008). Although haptophytes 5–10 μm and 10–20 μm in size made only a negligible contribution to the total haptophyte abundance, a higher abundance during the day compared to the night was found in the surface water and DCM layer. Studies have shown that mixotrophic haptophytes 3–5 μm in size removed more bacteria than cells >5 μm in size (Unrein *et al*., 2014; Chan *et al*., 2019). It is assumed that many haptophytes >5 μm in the present study are photoautotrophic, which are more sensitive to light conditions than the mixotrophic haptophytes. This may account for the higher abundance of haptophytes 5–10 μm and 10–20 μm in size observed during the day compared to the night. Furthermore, it is worth noting that most metabolism related to energy storage occurs during the day, which may account for the peak abundance of both total and nano-sized haptophyte biomass observed at 9:00 (Fig.6). However, it must be acknowledged that our survey was conducted for only 24 h. It is plausible that such a brief monitoring period might overlook valuable insights into the dynamics of the haptophyte community. Further study with a longer period might disclose more specific details.

4.2 Haptophytes Found in the Deep (200 m Depth) Water

Most previous studies on haptophytes have focused on the marine euphotic zone, including the surface water and DCM layer. Recent studies have identified mixotrophic activity in certain haptophyte groups, such as *Chrysochromulina* and *Prymnesium*. The mixotrophic nutritional mode provides haptophyte cells with an advantage over other phototrophic algae in certain environments, such as those with low light or with nutrient depletion, by obtaining carbon or phosphate through grazing. Through sampling haptophytes from both the surface and bottom (*ca*. 1% of the PAR of the surface euphotic zone) euphotic zones, Chan *et al*. (2019) determined that the abundances of haptophytes in the two depths were comparable and that the ingestion rates of haptophytes did not vary substantially between these two depths. Through the sampling period, the haptophyte abundance at 200 m depth in the present study remained constant at (46.4 ± 4.4) cells mL^{-1}, which is significantly lower than that in the surface water. Lack of light at 200 m in the current study might account for the discrepancy in haptophyte abundance between the present study and that of Chan *et al*. (2019). Studies have shown that *Prymnesium parvum* can endure for a certain duration in low light conditions, potentially owing in part to its mixotrophic activity (Brutemark and Granéli, 2011; Liu *et al*., 2016). At 200 m depth, the abundance and biomass of haptophytes do not exhibit any discernible rhythmicity. The absence of light at 200 m depth may impede the growth of certain phototrophic haptophyte groups, potentially accounting for the significantly reduced abundance of haptophytes in comparison to the surface water/DCM layer. A recent study by Xu *et al*. (2018) revealed the presence of eukaryotic phytoplankton cells in the deep western Pacific Ocean, and an analysis of the *psbA* gene transcripts revealed that haptophyte affiliated sequences, including *Prymnesium*, predominated. Therefore, the haptophyte cells observed at 200 m depth in the present study might consist of a combination of mixotrophic and phototrophic cells. The former may have survived by consuming prokaryotes and the latter by means of rapid sinking mechanisms (Xu *et al*., 2018). However, additional research is required to investigate the mixotrophic activity of haptophytes in the SCS, particularly in the deep waters, through the integration of TSA-FISH and grazing experiments.

4.3 Molecular Composition of Haptophyte Communities

Due to the high GC content in the haptophyte *SSU rRNA* gene, haptophytes were usually underrepresented in environmental surveys using universal eukaryotic primers targeting the *SSU rRNA* gene (Vaulot *et al*., 2002). Studies have shown that group-specific primers may be capable of recovering a greater diversity of the targeted groups (Liu *et al*., 2009). To obtain a preliminary understanding of the spatial and temporal dynamics of haptophytes in the SCS, the current study used general eukaryotic primers that targeted the V4 regions of the *SSU rRNA* gene, notwithstanding

the primers' limitations. The present study revealed that haptophyte sequences comprised a relatively minor fraction of eukaryotic sequences across all three water layers, with the maximum proportion (*ca*. 36.05%) observed at 21:00 in the surface water. Conversely, our observation did not find the highest cell abundance of haptophytes at this time point. This suggests that the relative abundance of sequences does not necessarily correspond to the true abundance of cells counted by FISH-TSA, as there are substantial differences in the *SSU rRNA* gene copy number among eukaryotic groups. *Chrysochromulina* species dominated haptophyte communities across all three water layers in the present study, whereas *Phaeocystis* species predominated the DCM communities. Using haptophyte specific primers, surveys of haptophytes in other oceanic regions, such as the Arctic Ocean, the Oslofjorden, the East China Sea, the Pacific Ocean, and the Tara Expedition's global survey of marine microorganisms, yielded comparable results (Egge *et al*., 2015; Gran-Stadniczeñko *et al*., 2017; Endo *et al*., 2018; Sun *et al*., 2022). The mixotrophic capability of *Chrysochromulina* species is widely recognized, particularly in environments with low light and nutrients (Kawachi *et al*., 1991). This characteristic confers on them an edge over pure phototrophic microalgae and enables them to thrive in the oceans (Liu *et al*., 2009; Penot *et al*., 2022). In the DCM layer, *Phaeocystis* species exhibit rapid growth due to the favorable light-nutrient balance, which at times even supersedes *Chrysochromulina* and dominates the haptophyte communities (Endo *et al*., 2018). Although lights were undetectable at 200 m depth, diverse haptophyte assemblages were still discovered from the RNA extracts. Given the fast-degrading rates of extracellular RNA, communities revealed by RNA-based sequencing were proposed to reflect the active members within the communities (Massana *et al*., 2015; Xu *et al*., 2017). The 200 m haptophyte communities were dominated by *Chrysochromulina* species, followed by environmental clades Prymnesiophyceae Clade_B3-E, and other groups. If the haptophyte communities identified at the 200 m depth in the present study do reflect the active members, we hypothesized that these cells were transported from the surface water *via* various fast sinking mechanisms, such as the formation of fecal pellets, and that some of them survived *via* phagotrophy. However, additional ingestion experiments were required to confirm this hypothesis. Furthermore, the lower contribution of environmental clades, including Prymnesiophyceae Clade_B3-E, to the haptophyte communities in the surface water and DCM layer compared to the 200 m depth suggests that these clades may have relied on phagotrophy as a means of survival. Further research is required to elucidate their identities (*e.g.*, morphology) and functions in the biogeochemical cycling that occurs in the water column, particularly in the deep, dark water.

4.4 Correlation Between Haptophyte Abundance and Environmental Variables

Environmental conditions play an important role in shaping the community composition and metabolic activity of haptophytes. Consistent with previous research, the abundance of the total haptophyte community and the 2–5 μm and 5–10 μm sized groups were found to be positively correlated with temperature and salinity and negatively correlated with the concentrations of nitrate, phosphate, and silicate (Endo *et al*., 2018). A significant portion of bacterivory in the global ocean is attributed to mixotrophic haptophytes (Unrein *et al*., 2014). Although we did not distinguish mixotrophic haptophytes from the total haptophyte community, our study revealed a strong correlation between the abundance of HPs and the abundance of 2–5 μm and 5–10 μm haptophytes. Prior studies have demonstrated that bacterivory of haptophytes primarily occurred within the size fraction of 2–10 μm (Unrein *et al*., 2014; Chan *et al*., 2019), and our results suggest that bacteria might serve as an important food source for mixotrophic haptophytes in the SCS. In the meantime, the abundance of VLPs and HNFs was positively correlated with haptophytes 2–5 μm and 5–10 μm in size, suggesting that VLPs and HNFs may exert top-down controls on small haptophytes through mechanisms such as viral lysis and grazing. It is important to acknowledge that the statistically significant correlations observed in this study do not necessarily imply the actual close relationships between haptophyte abundance and environmental parameters. Studies have shown that haptophyte abundance responds to various environmental variables. For example, in the East China Sea, haptophyte abundance was negatively correlated with temperature in spring, but did not correlate with nutrients (Lin *et al*., 2014). According to a monthly, year-round investigation conducted at the Blanes Bay Microbial Observatory on the Catalan coast, there was no significant correlation between haptophyte abundance and nutrients or available light parameters (Unrein *et al*., 2014). It is therefore reasonable to assume that intricate environmental factors influence the dynamics of haptophytes in the ocean. Future research that integrates the separation of function groups (*i.e.*, photoautotrophic and mixotrophic groups), measurements on comprehensive environmental parameters, and transcriptomic data will shed more light on the activity and driving mechanisms of haptophytes in diverse marine environments (Unrein *et al*., 2014; Chan *et al*., 2019; Kolody *et al*., 2019; Xie *et al*., 2022).

5 Conclusions

By applying FISH-TSA and high-throughput sequencing techniques, this study investigated the short-term dynamics of haptophyte abundance, cell size composition, and molecular community composition in three distinct water layers in the South China Sea: surface water, the DCM layer, and 200 m depth. Haptophyte communities in all three water layers were dominated by cells 2–5 μm in size. A higher abundance of small cells (< 2 μm and 2–5 μm) was observed during the night compared to that of the day time, whereas large cells (5–10 μm and 10–20 μm) were more prevalent during the day time. Members of *Chrysochromulina* and *Phaeocystis* predominated haptophyte communities, with the former being more abundant in the surface water and 200 m depth and the latter being more prevalent in the DCM layer. Close correlations between haptophyte abundance and multiple environmental biotic and abiotic

variables indicated that haptophyte communities in the ocean are probably shaped by complex environmental parameters, which needs further research due to their ubiquitous presence and flexible nutrition modes.

Acknowledgements

This work was supported by the National Natural Science Foundation of China (Nos. 42276095, 42188102, 42141003, and U20A20103), the Open Innovation Fund for Undergraduate Students of Xiamen University, and Ocean Negative Carbon Emissions (ONCE) program. We appreciate the assistance of Prof. Kuo-Ping Chiang and Dr. Yun-Chi Lin from Taiwan Ocean University with the FISH-TSA protocol, as well as Mr. Rong Gu and Mr. Wenxin Fan with sample collection.

References

Becker, K. W., Collins, J. R., Durham, B. P., Groussman, R. D., White, A. E., Fredricks, H. F., *et al*., 2018. Daily changes in phytoplankton lipidomes reveal mechanisms of energy storage in the open ocean. *Nature Communications*, **9** (1): 5179.

Becker, K. W., Harke, M. J., Mende, D. R., Muratore, D., Weitz, J. S., DeLong, E. F., *et al*., 2021. Combined pigment and metatranscriptomic analysis reveals highly synchronized diel patterns of phenotypic light response across domains in the open oligotrophic ocean. *The ISME Journal*, **15** (2): 520-533.

Bolger, A. M., Lohse, M., and Usadel, B., 2014. Trimmomatic: A flexible trimmer for Illumina sequence data. *Bioinformatics*, **30** (15): 2114-2120.

Børsheim, K. Y., and Bratbak, G., 1987. Cell volume to cell carbon conversion factors for a bacterivorous *Monas* sp. enriched from seawater. *Marine Ecology Progress Series*, **36**: 171-175.

Brutemark, A., and Granéli, E., 2011. Role of mixotrophy and light for growth and survival of the toxic haptophyte *Prymnesium parvum*. *Harmful Algae*, **10**: (4): 388-394.

Caron, D. A., Connell, P. E., Schaffner, R. A., Schnetzer, A., Fuhrman, J. A., Countway, P. D., *et al*., 2017. Planktonic food web structure at a coastal time-series site: I. Partitioning of microbial abundances and carbon biomass. *Deep Sea Research Part I: Oceanographic Research Papers*, **121**: 14-29.

Chan, Y. F., Chiang, K. P., Ku, Y., and Gong, G. C., 2019. Abiotic and biotic factors affecting the ingestion rates of mixotrophic nanoflagellates (Haptophyta). *Microbial Ecology*, **77**: 607-615.

Cuvelier, M. L., Allen, A. E., Monier, A., McCrow, J. P., Messié, M., Tringe, S. G., *et al*., 2010. Targeted metagenomics and ecology of globally important uncultured eukaryotic phytoplankton. *Proceedings of the National Academy of Sciences*, **107** (33): 14679-14684.

Durham, B. P., Boysen, A. K., Carlson, L. T., Groussman, R. D., Heal, K. R., Cain, K. R., *et al*., 2019. Sulfonate-based networks between eukaryotic phytoplankton and heterotrophic bacteria in the surface ocean. *Nature Microbiology*, **4**: 1706-1715.

Edgar, R. C., 2010. Search and clustering orders of magnitude faster than BLAST. *Bioinformatics*, **26**: 2460-2461.

Edgar, R. C., 2016a. UNOISE2: Improved error-correction for Illumina 16S and ITS amplicon sequencing. *BioRxiv*, 081257.

Edgar, R. C., 2016b. SINTAX: A simple non-Bayesian taxonomy classifier for 16S and ITS sequences. *BioRxiv*, 074161.

Edvardsen, B., Egge, E. S., and Vaulot, D., 2016. Diversity and distribution of haptophytes revealed by environmental sequencing and metabarcoding–A review. *Perspectives in Phycology*, **3** (2): 77-91.

Egge, E. S., Eikrem, W., and Edvardsen, B., 2015. Deep-branching novel lineages and high diversity of haptophytes in the Skagerrak (Norway) uncovered by 454 pyrosequencing. *Journal of Eukaryotic Microbiology*, **62** (1): 121-140.

Eller, G., Töbe, K., and Medlin, L. K., 2007. Hierarchical probes at various taxonomic levels in the Haptophyta and a new division level probe for the Heterokonta. *Journal of Plankton Research*, **29** (7): 629-640.

Endo, H., Ogata, H., and Suzuki, K., 2018. Contrasting biogeography and diversity patterns between diatoms and haptophytes in the central Pacific Ocean. *Scientific Reports*, **8** (1): 10916.

Gran-Stadniczeñko, S., Šupraha, L., Egge, E. D., and Edvardsen, B., 2017. Haptophyte diversity and vertical distribution explored by 18S and 28S ribosomal RNA gene metabarcoding and scanning electron microscopy. *Journal of Eukaryotic Microbiology*, **64** (4): 514-532.

Guillou, L., Bachar, D., Audic, S., Bass, D., Berney, C., Bittner, L., *et al*., 2012. The protist ribosomal reference database (PR^2): A catalog of unicellular eukaryote small sub-unit rRNA sequences with curated taxonomy. *Nucleic Acids Research*, **41** (D1): D597-D604.

Hammer, Ø., and Harper, D. A., 2001. Past: Paleontological statistics software package for educaton and data anlysis. *Palaeontologia Electronica*, **4** (1): 1.

Hernández Limón, M. D., Hennon, G. M., Harke, M. J., Frischkorn, K. R., Haley, S. T., and Dyhrman, S. T., 2020. Transcriptional patterns of *Emiliania huxleyi* in the North Pacific Subtropical Gyre reveal the daily rhythms of its metabolic potential. *Environmental Microbiology*, **22** (1): 381-396.

Hu, S. K., Connell, P. E., Mesrop, L. Y., and Caron, D. A., 2018. A hard day's night: Diel shifts in microbial eukaryotic activity in the North Pacific Subtropical Gyre. *Frontiers in Marine Science*, **5**: 351.

Kameyama, S., Otomaru, M., McMinn, A., and Suzuki, K., 2020. Ice melting can change DMSP production and photosynthetic activity of the haptophyte *Phaeocystis antarctica*. *Journal of Phycology*, **56** (3): 761-774.

Kawachi, M., Inouye, I., Maeda, O., and Chihara, M., 1991. The haptonema as a food-capturing device: Observations on *Chrysochromulina hirta* (Prymnesiophyceae). *Phycologia*, **30** (6): 563-573.

Kolody, B. C., McCrow, J. P., Allen, L. Z., Aylward, F. O., Fontanez, K. M., Moustafa, A., *et al*., 2019. Diel transcriptional response of a California Current plankton microbiome to light, low iron, and enduring viral infection. *The ISME Journal*, **13** (11): 2817-2833.

Lambert, S., Tragin, M., Lozano, J. C., Ghiglione, J. F., Vaulot, D., Bouget, F. Y., *et al*., 2019. Rhythmicity of coastal marine picoeukaryotes, bacteria and archaea despite irregular environmental perturbations. *The ISME Journal*, **13** (2): 388-401.

Landa, M., Turk-Kubo, K. A., Cornejo-Castillo, F. M., Henke, B. A., and Zehr, J. P., 2021. Critical role of light in the growth and activity of the marine N_2-fixing UCYN-A symbiosis. *Frontiers in Microbiology*, **12**: 666739.

Le Bouteiller, A., and Herbland, A., 1982. Diel variation of chlorophyll *a* as evidenced from a 13-day station in the equatorial Atlantic Ocean. *Oceanologica Acta*, **5**: (4): 433-441.

Li, Q. P., Hansell, D. A., and Zhang, J. Z., 2008. Underway monitoring of nanomolar nitrate plus nitrite and phosphate in oligotrophic seawater. *Limnology and Oceanography: Methods*, **6** (7): 319-326.

Li, R., Hu, C., Wang, J., Sun, J., Wang, Y., Jiao, N., *et al*., 2021.

Biogeographical distribution and community assembly of active protistan assemblages along an estuary to a basin transect of the northern South China Sea. *Microorganisms*, **9** (2): 351.

Lin, Y. C., Chung, C. C., Gong, G. C., and Chiang, K. P., 2014. Diversity and abundance of haptophytes in the East China Sea. *Aquatic Microbial Ecology*, **72** (3): 227-240.

Liu, H., Probert, I., Uitz, J., Claustre, H., Aris-Brosou, S., Frada, M., *et al*., 2009. Extreme diversity in noncalcifying haptophytes explains a major pigment paradox in open oceans. *Proceedings of the National Academy of Sciences*, **106** (31): 12803-12808.

Liu, Z., Campbell, V., Heidelberg, K. B., and Caron, D. A., 2016. Gene expression characterizes different nutritional strategies among three mixotrophic protists. *FEMS Microbiology Ecology*, **92** (7): fiw106.

Magoč, T., and Salzberg, S. L., 2011. FLASH: Fast length adjustment of short reads to improve genome assemblies. *Bioinformatics*, **27** (21): 2957-2963.

Marie, D., Partensky, F., Vaulot, D., and Brussaard, C., 1999. Enumeration of phytoplankton, bacteria, and viruses in marine samples. *Current Protocols in Cytometry*, **11**: Unit 11.11.

Marie, D., Shi, X. L., Rigaut-Jalabert, F., and Vaulot, D., 2010. Use of flow cytometric sorting to better assess the diversity of small photosynthetic eukaryotes in the English Channel. *FEMS Microbiology Ecology*, **72** (2): 165-178.

Mas, S., Roy, S., Blouin, F., Mostajir, B., Therriault, J. C., Nozais, C., *et al*., 2008. Diel variations in optical properties of *Imantonia rotunda* (Haptophyceae) and *Thalassiosira pseudonana* (Bacillariophyceae) exposed to different irradiance levels. *Journal of Phycology*, **44** (3): 551-563.

Masquelier, S., Foulon, E., Jouenne, F., Ferréol, M., Brussaard, C. P., and Vaulot, D., 2011. Distribution of eukaryotic plankton in the English Channel and the North Sea in summer. *Journal of Sea Research*, **66** (2): 111-122.

Massana, R., Gobet, A., Audic, S., Bass, D., Bittner, L., Boutte, C., *et al*., 2015. Marine protist diversity in European coastal waters and sediments as revealed by high-throughput sequencing. *Environmental Microbiology*, **17** (10): 4035-4049.

Morimoto, D., Šulčius, S., Tominaga, K., and Yoshida, T., 2020. Predetermined clockwork microbial worlds: Current understanding of aquatic microbial diel response from model systems to complex environments. *Advances in Applied Microbiology*, **113**: 163-191.

Not, F., Latasa, M., Scharek, R., Viprey, M., Karleskind, P., Balagué, V., *et al*., 2008. Protistan assemblages across the Indian Ocean, with a specific emphasis on the picoeukaryotes. *Deep Sea Research Part I: Oceanographic Research Papers*, **55** (11): 1456-1473.

Not, F., Massana, R., Latasa, M., Marie, D., Colson, C., Eikrem, W., *et al*., 2005. Late summer community composition and abundance of photosynthetic picoeukaryotes in Norwegian and Barents Seas. *Limnology and Oceanography*, **50** (5): 1677-1686.

Not, F., Simon, N., Biegala, I. C., and Vaulot, D., 2002. Application of fluorescent *in situ* hybridization coupled with tyramide signal amplification (FISH-TSA) to assess eukaryotic picoplankton composition. *Aquatic Microbial Ecology*, **28** (2): 157-166.

Penot, M., Dacks, J. B., Read, B., and Dorrell, R. G., 2022. Genomic and meta-genomic insights into the functions, diversity and global distribution of haptophyte algae. *Applied Phycology*, **3** (1): 340-359.

Reinfelder, J. R., 2011. Carbon concentrating mechanisms in eukaryotic marine phytoplankton. *Annual Review of Marine Science*, **3**: 291-315.

Schloss, P. D., Westcott, S. L., Ryabin, T., Hall, J. R., Hartmann, M., Hollister, E. B., *et al*., 2009. Introducing mothur: Open-source, platform-independent, community-supported software for describing and comparing microbial communities. *Applied and Environmental Microbiology*, **75** (23): 7537-7541.

Simon, N., Campbell, L., Örnolfsdottir, E., Groben, R., Guillou, L., Lange, M., *et al*., 2000. Oligonucleotide probes for the identification of three algal groups by dot blot and fluorescent whole-cell hybridization. *Journal of Eukaryotic Microbiology*, **47** (1): 76-84.

Stoeck, T., Bass, D., Nebel, M., Christen, R., Jones, M. D., Breiner, H. W., *et al*., 2010. Multiple marker parallel tag environmental DNA sequencing reveals a highly complex eukaryotic community in marine anoxic water. *Molecular Ecology*, **19**: 21-31.

Sun, P., Liao, Y., Wang, Y., Yang, E. J., Jiao, N., Lee, Y., *et al*., 2022. Contrasting community composition and co-occurrence relationships of the active pico-sized haptophytes in the surface and subsurface chlorophyll maximum layers of the Arctic Ocean in summer. *Microorganisms*, **10** (2): 248.

Tsuji, Y., and Yoshida, M., 2017. Biology of haptophytes: Complicated cellular processes driving the global carbon cycle. In: *Advances in Botanical Research*. Kader, J. C., and Delseny, M., eds., Academic Press, **84**: 219-261.

Turk-Kubo, K. A., Mills, M. M., Arrigo, K. R., van Dijken, G., Henke, B. A., Stewart, B., *et al*., 2021. UCYN-A/haptophyte symbioses dominate N_2 fixation in the Southern California Current System. *ISME Communications*, **1** (1): 42.

Unrein, F., Gasol, J. M., Not, F., Forn, I., and Massana, R., 2014. Mixotrophic haptophytes are key bacterial grazers in oligotrophic coastal waters. *The ISME Journal*, **8** (1): 164-176.

Vaulot, D., Romari, K., and Not, F., 2002. Are autotrophs less diverse than heterotrophs in marine picoplankton? *Trends in Microbiology*, **10** (6): 266-267.

Xie, Z. X., Yan, K. Q., Kong, L. F., Gai, Y. B., Jin, T., He, Y. B., *et al*., 2022. Metabolic tuning of a stable microbial community in the surface oligotrophic Indian Ocean revealed by integrated meta-omics. *Marine Life Science & Technology*, **4** (2): 277-290.

Xu, D., Li, R., Hu, C., Sun, P., Jiao, N., and Warren, A., 2017. Microbial eukaryote diversity and activity in the water column of the South China Sea based on DNA and RNA high throughput sequencing. *Frontiers in Microbiology*, **8**: 1121.

Xu, D., Sun, P., Zhang, Y., Li, R., Huang, B., Jiao, N., *et al*., 2018. Pigmented microbial eukaryotes fuel the deep sea carbon pool in the tropical Western Pacific Ocean. *Environmental Microbiology*, **20** (10): 3811-3824.

(Edited by Qiu Yantao)